

This coupling characteristic is favourable to simplify the fibre-coupling assembly in an optical measurement system, and is effective for cost reduction and miniaturisation.

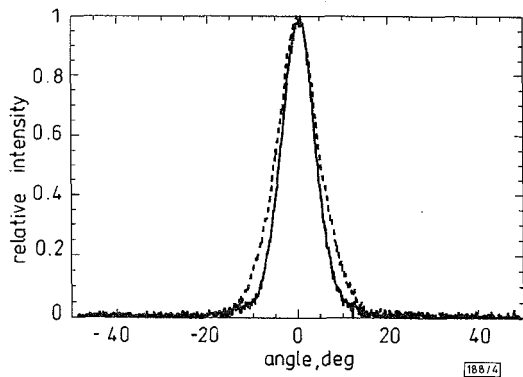


Fig. 4 Far-field patterns (FFPs) of NB-SLD

— horizontal FFP  
 - - - vertical FFP

**Acknowledgments:** We would like to thank Y. Tohmori, Y. Suzuki, O. Mitomi, I. Kotaka, K. Kasaya, K. Magari, Y. Noguchi, K. Kawano, H. Yasaka, and J. Yoshida for their technical discussions and encouragement.

© IEE 1997

5 February 1997

Electronics Letters Online No: 19970501

H. Okamoto, M. Wada, Y. Sakai, Y. Kawaguchi, Y. Kondo, Y. Kadota, K. Kishi and Y. Itaya (NTT Opto-electronics Laboratories, 3-1 Morinosato Wakamiya, Atsugi-shi, Kanagawa, 243-01 Japan)

## References

- LEE, T.P., BURRUS, C.A., and MILLER, B.I.: 'A stripe-geometry double-heterostructure amplified-spontaneous-emission (superluminescent) diode', *IEEE J. Quantum Electron.*, 1973, **9**, pp. 820–828
- BOHM, K., MARTEN, P., PETERMANN, K., WEIDEL, E., and ULRICH, R.: 'Low-drift fibre gyro using a superluminescent diode', *Electron. Lett.*, 1981, **17**, pp. 352–353
- TAKADA, K., YOKOHAMA, I., CHIDA, K., and NODA, J.: 'New measurement system for fault location in optical waveguide devices based on an interferometric technique', *Appl. Opt.*, 1987, **26**, (9), pp. 1603–1606
- NAGAI, H., NOGUCHI, Y., and SUDO, S.: 'High-power, high-efficiency 1.3 $\mu\text{m}$  superluminescent diode with a buried bent absorbing guide structure', *Appl. Phys. Lett.*, 1989, **54**, (18), pp. 1719–1721
- KWONG, N.S.K., BAR-CHAIM, N., and CHEN, T.: 'High-power 1.3 $\mu\text{m}$  superluminescent diode', *Appl. Phys. Lett.*, 1989, **54**, pp. 298–300
- NOGUCHI, Y., YASAKA, H., MIKAMI, O., and NAGAI, H.: 'High-power, broadband InGaAsP superluminescent diode emitting at 1.5 $\mu\text{m}$ ', *J. Appl. Phys.*, 1990, **67**, pp. 2665–2667
- TOHMORI, Y., SUZAKI, Y., OOHASHI, H., SAKAI, Y., KONDO, Y., OKAMOTO, H., OKAMOTO, M., KADOTA, Y., MITOMI, O., ITAYA, Y., and SUGIE, T.: 'High temperature operation with low-loss coupling to fibre for narrow-beam 1.3 $\mu\text{m}$  lasers with butt-jointed selective grown spot-size converter', *Electron. Lett.*, 1995, **31**, pp. 1838–1840
- OKAMOTO, H., SUZAKI, Y., TOHMORI, Y., OKAMOTO, M., KONDO, Y., KADOTA, Y., YAMAMOTO, M., KISHI, K., SAKAI, Y., WADA, M., and ITAYA, Y.: '1.3 $\mu\text{m}$  laser diodes with butt-jointed selectively grown spot-size converters uniformly fabricated on a 2-inch InP substrate', *Electron. Lett.*, 1996, **32**, pp. 1099–1101
- YOSHIDA, J., KAWACHI, M., SUGIE, T., HORIGUCHI, M., ITAYA, Y., and FUKUDA, M.: 'Strategy for developing low-cost optical modules for the ONU of optical subscriber systems'. Conf. Proc. VII Int. Workshop on Optical Access Networks (OAN), 1995, Paper VI-6.1
- KAMINOW, I.P., EISENSTEIN, G., and STULZ, L.W.: 'Measurement of the modal reflectivity of an antireflection coating on a superluminescent diode', *IEEE J. Quantum Electron.*, 1983, **19**, pp. 493–495

## Threshold and timing errors of 1 bit/2 level digital correlators in Earth observation synthetic aperture radiometry

A. Camps, F. Torres, I. Corbella, J. Bara and J.A. Lluch

Indexing terms: Radiometry, Remote sensing, Correlators

Analytical expressions for the errors generated in 1 bit/2-level digital correlators (1B/2L) are derived: threshold errors in comparators and timing (skew and jitter) errors in samplers. These expressions are used to specify the parameters of the comparators and samplers in high performance 1B/2L digital correlators that are required in Earth observation synthetic aperture radiometry.

**Introduction:** Future Earth observation missions to monitor soil moisture and ocean salinity may use synthetic aperture radiometry at low frequencies (1.400–1.427 MHz) [1, 2]. Brightness temperature maps are formed by processing the cross-correlations of the signals collected by a sparse array of small antennas. As suggested in [1], the simultaneous computation of a large number of cross-correlations can be performed in space-borne interferometric radiometers by means of 1 bit/2-level (1B/2L) digital correlators, despite their lower radiometric sensitivity. Their main advantages are their simplicity (a threshold comparator/sampler insensitive to signal amplitude, a NOT-XOR gate as a multiplier and a counter as an integrator), low power consumption, ease of integration and their simple signal distribution network. This Letter focuses on the errors generated in the measurement of the cross-correlation  $\mu$  by means of 1B/2L digital correlators as

$$\mu = \frac{E[i_1(t)i_2(t)]}{\sqrt{E[i_1(t)i_1(t)]E[i_2(t)i_2(t)]}} + j \frac{E[q_1(t)i_2(t)]}{\sqrt{E[q_1(t)q_1(t)]E[i_2(t)i_2(t)]}} \quad (1)$$

where  $i_{1,2}(t)$  and  $q_{1,2}(t)$  are the in-phase and quadrature components of the narrowband radiation collected by the antennas. The cross-correlation  $\mu$  is obtained from an intermediate correlation  $Z = Z_r + jZ_j$ . Its real and imaginary parts are  $Z_r = E[\text{sign}(i_1(t))\text{sign}(i_2(t))]$  and  $Z_j = E[\text{sign}(q_1(t))\text{sign}(i_2(t))]$ , i.e. the ratio of the coincidences between the sign of the samples of the components  $i_1(t)$ ,  $i_2(t)$  and  $q_1(t)$ ,  $i_2(t)$ , respectively. In the absence of errors, the cross-correlation  $\mu_{r,j}$  and the intermediate correlation  $Z_{r,j}$  are related by the well known expression [3, 4]

$$Z_{r,j} = \frac{2}{\pi} \arcsin(\mu_{r,j}) \quad (2)$$

According to eqns. 41 and 43 of [3], this equation holds with an accuracy of better than  $10^{-4}$  over the range  $|\mu| < 0.1$  [1], when the effect of the transfer function of the comparators that clips the signal at a level  $c$  is  $< 2 \times 10^{-4}$ . The clipping factor  $c$  is defined as the ratio between the clipping amplitude and  $\sigma$ , the original RMS amplitude of the signals being correlated. Thus, for an RMS amplitude of 220 mV, the clipping amplitude must be  $< 2$  mV, a value that can be achieved with high speed comparators [5].

**Evaluation of comparator threshold errors:** We define  $b_1(t)$  and  $b_2(t)$  as two joint Gaussian functions equal to  $b_1(t) \triangleq i_1(t)$ ,  $b_2(t) \triangleq i_2(t)$ , for  $Z_r$  and  $\mu_r$ , and  $b_1(t) \triangleq q_1(t)$ ,  $b_2(t) \triangleq i_2(t)$  for  $Z_j$  and  $\mu_j$  with the joint probability density function

$$f(b_1, b_2) = \frac{1}{2\pi\sigma^2\sqrt{1-\mu_{12}^2}} \exp\left(-\frac{b_1^2 + b_2^2 - 2b_1b_2\mu_{12}}{2\sigma^2(1-\mu_{12}^2)}\right) \quad (3)$$

In the presence of comparator threshold errors, the  $Z_{r,j}$  is computed as

$$Z_{r,j} = E[\text{sign}(b_1(t) - \Delta x_1)\text{sign}(b_2(t) - \Delta x_2)] \quad (4)$$

and the relationship between  $Z_{r,j}$  and  $\mu_{r,j}$  can be derived by means of Price's theorem [4] for  $g_{1,2}(x) = \text{sign}(x - \Delta x_i)$  and  $m = 1$

$$\begin{aligned} \partial^m \hat{Z}(\mu) / \partial \mu^m &= \sigma^{2m} E[\partial^m g_1 / \partial b_1^m \cdot \partial^m g_2 / \partial b_2^m] \\ &= 4\sigma^2 E[\delta(b_1(t) - \Delta x_1)\delta(b_2(t) - \Delta x_2)] \end{aligned}$$

$$= \frac{2}{\pi\sqrt{1-\mu_{12}^2}} \exp\left(-\frac{\Delta x_1^2 + \Delta x_2^2 - 2\Delta x_1\Delta x_2\mu_{12}}{2\sigma^2(1-\mu_{12}^2)}\right) \quad (5)$$

which leads to

$$\begin{aligned} \hat{Z}(\mu) &= 2/\pi \int_0^\mu \partial \hat{Z}(\mu)/\partial \mu d\mu + Z_{offset} \quad (6) \\ &\simeq 2/\pi \left[ \arcsin(\mu) - b + (a\mu + b)/\sqrt{1-\mu^2} \right] \\ &\quad + \operatorname{erf}(\Delta x_1/\sqrt{2}\sigma)\operatorname{erf}(\Delta x_2/\sqrt{2}\sigma) \end{aligned}$$

where

$$a \triangleq -(\Delta x_1^2 + \Delta x_2^2)/2\sigma^2 \quad b \triangleq \Delta x_1\Delta x_2/\sigma^2 \quad (7)$$

Note that eqn. 6 reduces to eqn. 2 if there are no threshold errors. Additional offset terms are generated by the presence of correlated noise, such as that caused by local oscillator leakage [6]. The offsets can be calibrated by measuring the correlation when the two antennas are switched to different matched loads that generate uncorrelated noise. The expected normalised visibility can be measured with an error  $< 10^{-4}$  for  $|\mu| < 0.1$  by means of the ideal nonlinear relationship

$$\hat{\mu}_{r,j}(\hat{Z}_{r,j}) = \sin(\pi/2 \hat{Z}_{r,j}(\mu_{r,j})) \simeq \mu_{r,j}(1 - a_{r,j}) \quad (8)$$

for an input power of 0dBm over 50Ω ( $\sigma = 220\text{mV}$ ) [6], and a comparator threshold error of  $\Delta x_{1,2} = 1.4\text{mV}$ , leading to an offset term  $Z_{offset} = 3 \times 10^{-5}$  and  $-a \simeq b \simeq 4 \times 10^{-4}$ . At this point it must be pointed out that  $\mu_r$  and  $\mu_j$  suffer from the different gain terms  $(1-a_r)$  and  $(1-a_j)$  that can be neglected by choosing  $\sigma/\Delta x_{1,2} > 100$ . The theoretical expressions have been checked by connecting a 50% duty cycle rectangular pulse train to the  $i_1(t)$  input and measuring the correlation with a 66MHz fast-TTL 1B/2L digital correlator prototype [6]. A rectangular pulse train has been selected due to the difficulty of generating correlated noise with the required accuracy ( $\epsilon_u < 10^{-4}$ ). The results are shown in Fig. 1. As predicted by eqns. 7 and 8, the error decreases for increasing  $\sigma/\Delta x_{1,2}$  ratios, reaches an optimum around 300–400mVpp (3–5dBm), and grows for larger  $\sigma/\Delta x_{1,2}$  ratios due to the saturation of the last amplifying stage. When correlating thermal noise, the signal power must be reduced to 0dBm to avoid amplifier saturation caused by the clipping of noise peaks.

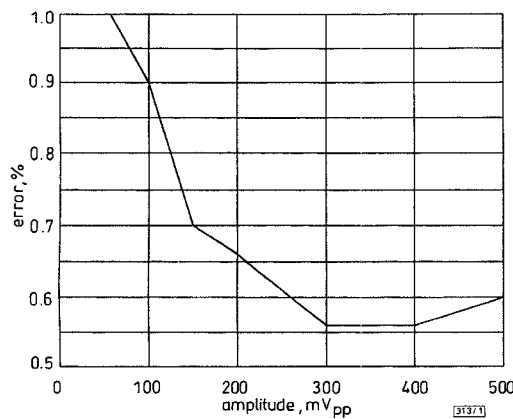


Fig. 1 Correlation error against amplitude of pulse train

Duty cycle 50%,  $f = 15\text{MHz}$

**Evaluation of timing errors:** To avoid re-radiation from the local oscillator to the antenna, signals are not usually down-converted to the baseband, i.e.  $f_i = f_o - f_{LO} \neq 0$ . In this case, the measured normalised correlation takes the form

$$\hat{\mu}_r(\tau) = \tilde{r}(-\tau)[\mu_r(0) \cos(2\pi f_I \tau) + \mu_j(0) \sin(2\pi f_I \tau)] \quad (9a)$$

$$\hat{\mu}_j(\tau) = \tilde{r}(-\tau)[\mu_j(0) \cos(2\pi f_I \tau) - \mu_r(0) \sin(2\pi f_I \tau)] \quad (9b)$$

where  $\tilde{r}(-\tau)$  is the so called fringe-washing function that takes into account decorrelation effects. Assuming that the receivers frequency response can be modelled by a Gaussian filter with noise bandwidth  $B$ , the fringe-washing function takes the form

$$\tilde{r}(-\tau) = F^{-1}[|H(f)|^2] = e^{-\pi B^2 \tau^2} \quad (10)$$

If the signals are sampled simultaneously at  $\tau = 0$ , the true cross-correlation  $\mu_{r,j}(0)$  is recovered from eqn. 9. In practice there are

sampling timing errors  $\tau = t_d + \Delta t$ , where  $t_d$  is a constant sampling skew between the two channels ( $i_1 - i_2$  or  $q_1 - i_2$ ) and  $\Delta t$  the jitter. Assuming that the jitter  $\Delta t$  is a zero-mean Gaussian random variable with standard deviation  $\sigma_\tau$ , the measured cross-correlation can be computed as

$$\hat{\mu}_r(\tau) = \langle \tilde{r}(-\tau)[\mu_r(0) \cos(2\pi f_I \tau) + \mu_j(0) \sin(2\pi f_I \tau)] \rangle_{\tau=t_d+\Delta t} \quad (11a)$$

$$\hat{\mu}_j(\tau) = \langle \tilde{r}(-\tau)[\mu_j(0) \cos(2\pi f_I \tau) - \mu_r(0) \sin(2\pi f_I \tau)] \rangle_{\tau=t_d+\Delta t} \quad (11b)$$

After some manipulations, eqn. 11 can be evaluated and simplified for the typical values involved  $-t_{\mu_{r,j}} < 2\text{ns}$ ,  $\sigma_{\mu_{r,j}} < 3\text{ns}$ ,  $f_0 = 1.410\text{MHz}$ ,  $f_{L0} = 1.395\text{MHz}$ ,  $f_1 \simeq f_0 - f_{L0}$  and  $B \simeq 30\text{MHz}$ :

$$\hat{\mu}_r \simeq e^{-\pi[2\pi(f_I \sigma_{\tau_r})^2 + (B t_{d_r})^2]} \operatorname{Real}[\mu_r(0) + j\mu_j(0)] e^{j2\pi f_I t_{d_r}} \quad (12a)$$

$$\hat{\mu}_j \simeq e^{-\pi[2\pi(f_I \sigma_{\tau_j})^2 + (B t_{d_j})^2]} \operatorname{Imag}[\mu_r(0) + j\mu_j(0)] e^{j2\pi f_I t_{d_j}} \quad (12b)$$

Note that the first term in eqn. 12 is the fringe-wash gain factor, which is  $\sim 0.95$  and may be slightly different for the real and the imaginary parts of the measured cross-correlation. Conversely, the phase term inside the brackets is a phase error different for each component  $\hat{\mu}_r$  and  $\hat{\mu}_j$ , that can be decomposed into an in-phase term and a quadrature error

$$\Phi^{in\ phase} = \frac{\Phi_r + \Phi_j}{2} = \pi f_I (t_{d_r} + t_{d_j}) < 10.8^\circ \quad (13)$$

$$\Phi^{quadrature} = \Phi_r - \Phi_j = 2\pi f_I (t_{d_r} - t_{d_j}) < 0.14^\circ$$

The quadrature error is very small and has a negligible impact over the radiometric accuracy [6]. However, the in-phase term must be very similar between all the correlations to allow simpler calibration techniques. That is, samplers are required to be matched with skews between sampling times of  $< 0.09\text{ns}$  to achieve a negligible non-separable phase error of  $|\phi_{m-n}^{in\ phase} - \phi_{p-q}^{in\ phase}| < 0.5^\circ$  between channels  $m-n$  and  $p-q$  [6]. Fig. 2 shows the measured relative error against the frequency of a 50% duty cycle rectangular pulse train connected to the  $i_1(t)$  input. Except for the lowest frequencies, where a DC block filter attenuates the signals, the error grows with frequency as predicted by eqn. 13.

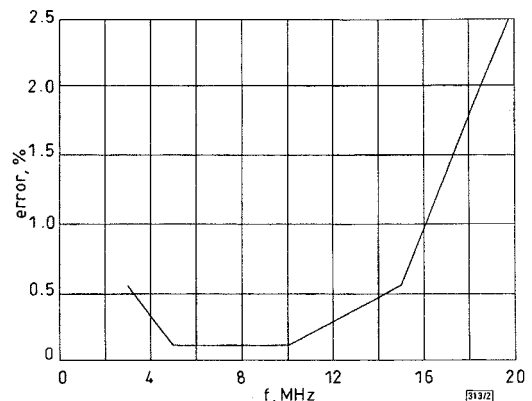


Fig. 2 Correlation error against frequency of pulse train

Duty cycle = 50%, Amplitude = 300 mVpp

**Conclusions:** Closed form expressions have been derived to evaluate the errors generated in 1B/2L digital correlators. In practice, clipping and threshold errors can be neglected with an error of  $< 10^{-4}$  provided that the clipping amplitude and the threshold errors are smaller than 2 and 1.4mV, respectively, for an input signal of 220mV<sub>eff</sub> (0dBm over 50Ω). However, the non-separable phase error introduced by skew sampling errors may be comparable to that introduced by filter mismatches [6] and must be taken into account when selecting the sampler technology. For a low-pass signal of 30MHz bandwidth, centred at 15MHz, sampling skews of  $< 0.09\text{ns}$  are required to neglect the non-separable phase errors.

**Acknowledgments:** This work has been partially supported by the Spanish Ministry of Education and Culture CICYT TIC 96/0879.

A. Camps, F. Torres, I. Corbella, J. Bara and J.A. Lluich (Department of Signal Theory and Communications, Universitat Politècnica de Catalunya, Campus Nord, Mòdul D4, c/Gran Capità s/n, 08034 Barcelona, Spain)

References

- MARTIN-NEIRA, M., MENARD, Y., GOUTOULE, J.M.M., and KRAFT, U.: 'MIRAS, a two-dimensional aperture synthesis radiometer'. Proc. Int. Geoscience Remote Sensing Soc. (IGARSS), 1994, pp. 1323–1325
- MARTIN-NEIRA, M., GOUTOULE, J.M., KNIGHT, A., CLAUDE, J., BARA, J., CAMPS, A., TORRES, F., CORBELLA, I., LANNES, A., ANTERRIEU, E., LAURSEN, B., and SKOU, N.: 'Integration of MIRAS breadboard and future activities'. Proc. Int. Geoscience Remote Sensing Soc. (IGARSS), 1996, pp. 869–871
- VAN VLECK, J.H., and MIDDLETON, D.: 'The spectrum of clipped noise'. Proc. IEEE, 1966, 54, (1), pp. 2–19
- HAGEN, J.B., and FARLEY, D.T.: 'Digital-correlation techniques in radio science', Radio Science, 1973, 8, (8–9), pp. 775–784
- MAXIMS MAX 905 and 915 data sheets
- CAMPS, A.: 'Application of interferometric radiometry to earth observation', Ph. D. Thesis, Polytechnic University of Catalonia, November 1996, chaps. 4 and 9

**AlGaIn/GaN double heterostructure channel modulation doped field effect transistors (MODFETs)**

Zhifang Fan, Changzhi Lu, A.E. Botchkarev, H. Tang, A. Salvador, Ö. Aktas, W. Kim and H. Morkoc

Indexing terms: MODFET, Semiconductor devices

AlGaIn/GaN double heterostructure channel modulation doped field effect-transistors (DHCMODFETs) with a 1.5–1.75µm gate length and a 3µm channel length exhibiting record transconductances and saturation current levels have been demonstrated. The maximum normalised drain current and transconductance are ~1100mA/mm and 270mS/mm, respectively, at room temperature. Near pinch-off, the drain breakdown voltage is ~80V. At an elevated temperature of 300°C, the maximum drain source current and extrinsic transconductance of the device are ~500mA/mm and 120mS/mm, respectively.

The high electron peak and saturation velocity and a large breakdown field attributes of GaN, combined with its good thermal conductivity and stability make it an attractive material for high power/temperature electronic devices [1, 2]. The wide bandgap of GaN leads to low intrinsic carrier concentration enabling a more precise control of free carrier concentration over a wide range of temperatures [3]. Recent investigations have led to the realisation of several AlGaIn/GaN field effect transistors [4–8]. Binari *et al.* [6] presented the results of DC measurements showing that these devices can operate at least up to 300°C while Khan *et al.* [7] and Aktas *et al.* [8] also reported in some detail the current voltage characteristics at temperatures up to 300°C. GaN based MODFETs have also been reported to exhibit microwave current gain cutoff frequencies approaching 40GHz at the 0.25µm gate length level [9], and RF power levels of 1W/mm at 2GHz [10] and 1.5W/mm at 4GHz [11]. In this Letter, we present a novel AlGaIn/GaN double heterostructure channel MODFET exhibiting a record DC performance which rivals that of other high performance III-V based MODFETs.

The layer structure of the DHCMODFET is shown in Fig. 1. The film was grown by reactive molecular beam epitaxy with ammonia as the nitrogen source [12]. The AlGaIn/GaN double heterostructure channel layer was grown on top of an undoped, highly resistive GaN layer. A 70Å GaN channel layer with an estimated background electron concentration of  $5 \times 10^{18} \text{cm}^{-3}$ , straddled by two 20Å thick *n*-AlGaIn with Si doping of  $1.3 \times 10^{19}$  and  $8.7 \times 10^{19} \text{cm}^{-3}$ , formed the core of the DHCMODFET. Separating

these two doped AlGaIn donor layers are two 20Å thick *i*-AlGaIn spacer layers adjacent to the channel layer. As in the case in AlGaAs/GaAs MODFETs, the sole purpose of the two AlGaIn spacer layers is to further separate the electrons from the donors. Lastly, a 30Å thick *i*-AlGaIn cap layer was grown on which to form the Schottky barrier gate. By Hall-effect measurement, the mobility and sheet carrier density in the 2D electron gas (2DEG) are found to be  $304 \text{cm}^2/\text{Vs}$  and  $3.7 \times 10^{13} \text{cm}^{-2}$ , respectively, at room temperature.

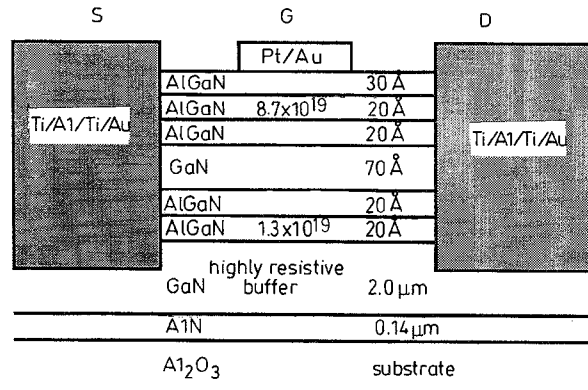


Fig. 1 Schematic diagram of AlGaIn/GaN double heterostructure MODFET layer structure used

A number of DHCMODFETs with gate lengths of 1.5–1.75µm and gate width of 40µm were fabricated on the same wafer. The details of the fabrication process are discussed elsewhere [5]. Briefly, reactive ion etching was used to isolate the devices, Ti/Al/Ti/Au (200/1200/400/100Å) was used to form the source and drain contacts and Pt/Au (300/700Å) was used for Schottky contacts.

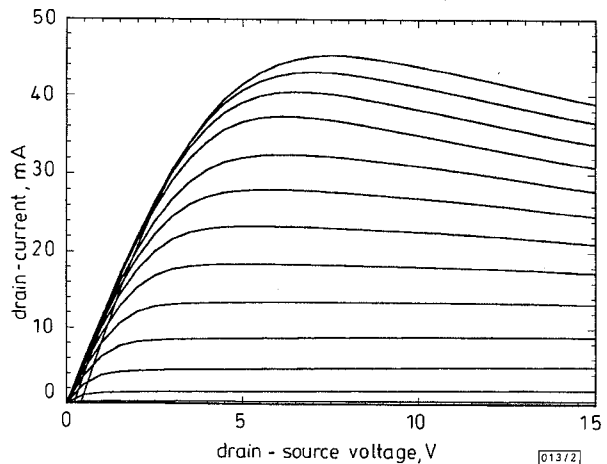


Fig. 2 Output I-V characteristics of AlGaIn/GaN double heterostructure MODFET at room temperature for gate biases of +3.5 to -4V with 0.5V steps

$V_g = 3.5 \text{V}$ ,  $T = \text{RT}$

The DC drain characteristics at room temperature of the DHCMODFET device with gate length of 1.5µm, gate width of 40µm, and drain source separation of 3µm are presented in Fig. 2. The maximum drain source current  $I_{DS}$  corresponding to a drain-source voltage  $V_{DS} = 7 \text{V}$ ,  $V_{GS} = 3.5 \text{V}$  is ~1100mA/mm which compares with the maximum  $I_{DS}$  value of 695mA/mm obtained for a MODFET reported earlier [5]. The DHCMODFET has a room temperature extrinsic transconductance  $g_m = 270 \text{mS/mm}$  which compares with a value of 220mS/mm reported earlier [5]. The value of the total resistance  $R_T$  extracted from the linear region of the I-V curves is 4 Ω/mm. Near pinch-off, the drain breakdown voltage is ~80V, indicating excellent power potential of the device.

The I-V characteristics of the DHCMODFET at 300°C is shown in Fig. 3. These measurements were made in a nitrogen pressurised container to avoid possible oxidation of the contacts and probes. The maximum drain-source current and extrinsic transconductance of the DHCMODFET are 500mA/mm and 120mS/mm, respectively. From Figs. 2 and 3 it can also be seen